Molecular Dynamics Study on the Effect of Chain Branching on the Physical Properties of Lipid Bilayers: Structural Stability

Wataru Shinoda,*,† Masuhiro Mikami,† Teruhiko Baba,‡ and Masakatsu Hato‡

Research Institute for Computational Sciences (RICS), National Institute of Advanced Industrial Science and Technology (AIST), Central-2, Umezono 1-1-1, Tsukuba 305-8568, Japan, and Nanotechnology Research Institute (NRI), National Institute of Advanced Industrial Science and Technology (AIST), Central-5, Higashi 1-1-1, Tsukuba 305-8565, Japan

Received: May 29, 2003; In Final Form: September 10, 2003

In general, bilayers composed of branch-chained lipid molecules are known to have high stability and low ion permeability. To understand how chain branching affects bilayer properties on a molecular level, two molecular dynamics (MD) simulations of lipid bilayers have been undertaken in the isothermal−isobaric ensemble. The first MD simulation was carried out on the straight-chained DPPC bilayer, and the second was carried out on the branch-chained DPhPC bilayer. Chain branching reduced segmental order of the lipid chain. This would be closely related to a high gauche probability at the dihedrals in the vicinity of *tert*-carbons; these dihedrals brought about the chain bending at the branched segments. Due to the characteristic conformation of the branched chain, some different effects were observed: First, the probability of parallel orientation of the two chains in a lipid was reduced; second, a chain caught between the two chains of the neighboring lipid in the same leaflet of the bilayer was frequently observed. As a consequence, the branched chain showed a much lower overall rate of trans−gauche isomerization than its straight counterpart. In conclusion, the high structural stability of the branched DPhPC bilayer is attributable mainly to the slow conformational motion of the hydrophobic chain, which is clearly correlated with the observed chain "entrapment" between the lateral neighboring lipid molecules.

1. Introduction

Lipid molecules, which are the most essential component of biological membranes, play an important role in determining membrane stability and function. A slight structural variation in lipid molecules sometimes produces dramatic changes in the bilayer properties, such as structural stability and solute permeability.[1] For example, it was shown that lipids bearing highly branched hydrophobic chains form a stable bilayer with low permeability to proton and other ionic or nonionic solutes.[2] Highly branched lipids were found from archaea, which inhabit extreme conditions such as very high temperature, low pH, and high salt concentrations. Based on empirical knowledge, some of the present authors have synthesized novel model archaeal lipids, i.e., branch-chained glycolipids,[3] to develop stable bilayer matrixes for membrane proteins[4] and reported bilayers composed of this type of lipids actually exhibit stability to external field fluctuations[5] and low permeability to proton and other ionic solutes.[5,6] The effect of chain branching on the bilayer properties at the molecular level has not, however, been well understood.

In addition to the novel branch-chained glycolipids, a synthetic model archaeal phospholipid 1,2-diphytanoyl-*sn*-glycero-3-phosphocholine (DPhPC), which forms a liquid-crystalline bilayer structure in the presence of excess water at a wide temperature range, from −120 to 120 °C,[7] has been more extensively employed as a reconstitution matrix for channel-forming peptides and/or proteins due to its high stability.[8] Figure 1 depicts the molecular structure of the DPhPC molecule, together with its straight-chained counterpart, 1,2-dipalmitoyl-*sn*-glycero-3-phosphocholine (DPPC). DPhPC and DPPC each have hydrophobic main chains consisting of 16 carbons; DPhPC has four additional methyl groups, which are attached at the 3rd, 7th, 11th, and 15th carbons along the main chain.

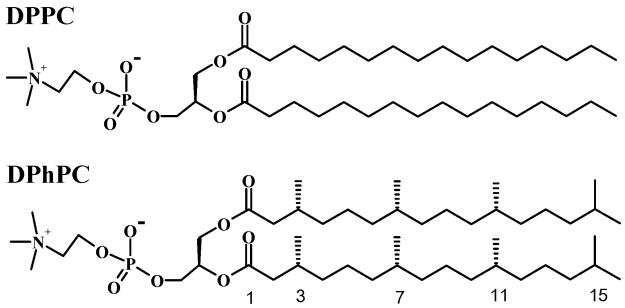

Figure 1. Chemical structures of DPPC and DPhPC.

In this study, two molecular dynamics (MD) simulations were undertaken to investigate the effect of lipid chain branching on bilayer properties. The first simulation was carried out on the straight-chained DPPC and the second on the branch-chained DPhPC. Both MD simulations were performed under the same thermodynamic conditions, fulfilled by the isothermal−isobaric ensemble technique, to extract the essential changes that chain branching causes in the liquid-crystalline bilayer properties. In this work, we investigated the structure and dynamics of these lipid bilayers in relation to chain branching's effect on their structural stability. In the following, after briefly describing the model in section 2, we present the results of the MD calculations

* To whom correspondence should be addressed. Phone: +81-29-861-6251. Fax: +81-29-851-5426. E-mail: w.shinoda@aist.go.jp.
† RICS.
‡ NRI.

10.1021/jp035493j CCC: $25.00
Published on Web 11/21/2003

and our analyses in section 3. Finally, the main conclusions are summarized.

2. Methods

2.1. Force Field and System Setup. DPPC and DPhPC molecules were modeled by the CHARMM force field (PARM27)[9] with modified rigid TIP3P water.[10] Each bilayer system was composed of 72 lipid molecules, each of which was hydrated by 29 water molecules (2088 water molecules in total). Initial conformation of the DPPC and DPhPC molecules was constructed on the basis of the crystalline DMPC structure obtained by X-ray diffraction measurement.[12] Lipid molecules were packed into a bilayer, in which each molecule occupied a cross-sectional area corresponding to the experimental value. In the first 500 ps, to enhance chain melting, MD calculation was performed at a high temperature, 353 K, in the NP_nAT ensemble, in which the cell vectors **a** and **b** were fixed and only vector **c** was a dynamic variable. Here we set the bilayer on the **ab** plane. Another 500 ps MD was used to equilibrate the system at 323 K in the NPT ensemble with the fully flexible cell.

2.2. Molecular Dynamics Simulations. To generate the isothermal−isobaric (NPT) ensemble, the fully flexible cell with the modularly invariant momentum form was employed as the barostat, and the Nosé−Hoover chain (length = 5) was used as the thermostat.[13] The response times of the barostat and thermostat were set to 2 and 0.5 ps, respectively. The equations of motion were integrated by the rRESPA algorithm.[14] After the equilibration MD run, a 1.5 ns NPT-MD simulation was carried out for each system under the same thermodynamic conditions: $P = 0.1$ MPa and $T = 323$ K (in the liquid-crystal phase). Although several experimental measurements on the DPhPC bilayer were undertaken at 298 K, we chose the rather high temperature of 323 K to investigate the effect of chain branching on the bilayer properties under the same thermodynamic conditions. The Lennard-Jones interactions were truncated by applying a smooth switching function to the potential over the range of 10−12 Å. Electrostatic interactions were calculated with the Ewald method.[11] All bond lengths involving hydrogen atoms were fixed by using the SHAKE/ROLL and RATTLE/ROLL procedure.[13] This allowed us to use a time step of 2 fs. By choosing 10^{-8} as the relative tolerance of the fixed bond length of the SHAKE procedure, we obtained accurate trajectories in the course of the MD runs; no global drift of the conserved quantity was observed and the relative error was kept to within 5×10^{-4}. MD simulations and all analyses have been carried out on a 16-node AlphaStation XP1000 (600 MHz) using the MD simulation tool MPDyn,[15] in which parallel directives were implemented using the public domain Message Passing Interface (MPI).

3. Results and Discussion

3.1. Bilayer Dimensions. To assess the convergence of the simulated system to the equilibrium state, several structural and energetic quantities were monitored. Figure 2 plots the time evolution of the cross-sectional area per lipid. Since the cross-sectional area usually provides a more detailed view of convergence than do other bulk quantities, such as volume and internal energy,[16] it is sometimes used to measure how well equilibrated the simulated system is. Figure 2 reveals that both DPPC and DPhPC bilayers reached the stable state with respect to the cross-sectional area. The areas averaged over the 1.5 ns MD trajectories were 62.0 Å^2 in DPPC and 76.8 Å^2 in DPhPC membranes, both of which were in good agreement with those

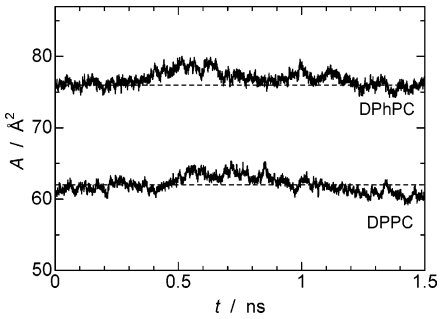

Figure 2. Time evolution of average cross-sectional area per lipid during the production runs. Dashed lines indicate experimental values.[17,18]

TABLE 1: Comparison of the Structural Data with Experimental Measurements[a]

	DPPC		DPhPC	
	MD	expt	MD	expt
D	68.2	67[b]	60.5	
d_{P-P}	39.6	39.6[b]	38.2	38[d]
A	62.0	62.9[b]	76.8	76[d]
gauche	27	25−36[c]	31	

[a] *D*, lamella repeat distance [Å]; d_{P-P}, peak-to-peak distance of the electron density profile along the bilayer normal [Å]; *A*, cross-sectional area [Å^2]; gauche, averaged gauche fraction in the hydrophobic chains [%]. [b] Experimental data are taken from ref 17. [c] Experimental data are taken from ref 19. [d] Experimental data (at 298 K) are taken from ref 18.

obtained by experimental measurements (Table 1). While the difference in the cross-sectional area between DPPC and DPhPC was as large as about 15 Å^2, the peak-to-peak distance of the electron density profile (i.e., membrane thickness) showed no significant change (39.6 Å in DPPC, 38.2 Å in DPhPC membrane). These were also in good agreement with the experimental values (Table 1). All of the other monitored quantities, such as potential energy, lamella repeat spacing, and average probability of gauche conformers over the hydrophobic chains, were also well converged during the equilibration run, and showed only slight fluctuations around the average values during the production run.

3.2. Chain Orientation. Figure 3a shows the distribution of angles between the chain vector and the bilayer normal. The chain vector was defined as the vector connecting C1 (carbonyl carbon) and C15, and the bilayer normal vector was directed to the outside of the membrane. Figure 3 demonstrates that the chain orientation parallel to the bilayer normal was most probable in both the DPPC and DPhPC membranes. However, the distribution of DPhPC was slightly broader than that of DPPC. In their MD simulation, Husslein et al.[20] observed some DPhPC chains parallel to the bilayer plane.[21] They actually found a bimodal distribution of the angles between the chain vector and the bilayer normal, with the second peak located at about 90°, although the probability corresponding to the second peak was small. In the present study, however, we did not observe a bimodal distribution, only a slightly broader distribution of angles for the branch-chained DPhPC.

The calculated distribution of the angles between the two chain vectors in a lipid molecule is shown in Figure 3b. The difference between the two lipid molecules was clear in this case. Two parallel chains appeared most frequently for both lipid molecules, as was also reported by the previous MD study.[16] The DPhPC molecule, however, showed a significantly broader distribution of angles. This suggested that hydrophobic chains of DPhPC molecules are likely to be interposed between

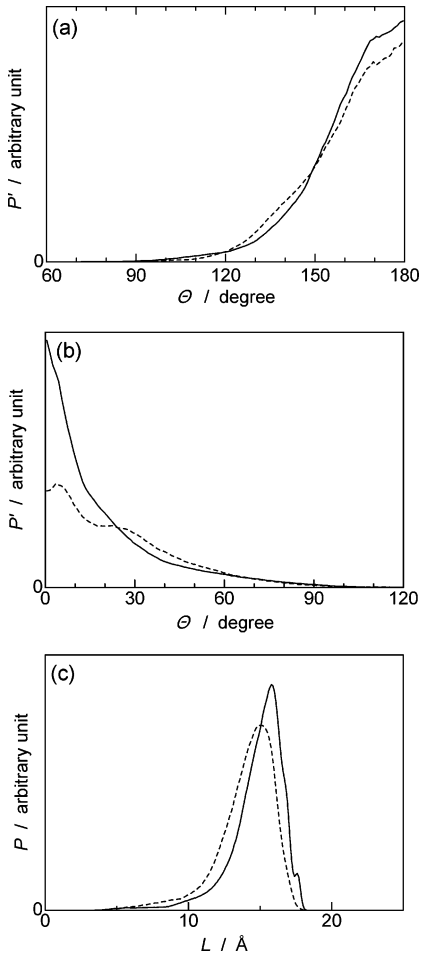

Figure 3. (a) Distribution of angles between the chain vector and the bilayer normal. (b) Distribution of the angles between the two chain vectors in a lipid molecule. (c) Probability distribution of the length of the chain vector. The chain vector was defined as the vector connecting C1 (carbonyl carbon) to C15. Solid line, DPPC; dashed line, DPhPC. The volume weight was taken into account in the distribution function ($P' = P/\sin\theta$).

the two hydrophobic chains of the lateral neighboring lipid molecules. This is clearly shown in Figure 4, which presents typical snapshots of patches of the lipid layers. It is clear that some chains exist between the two chains of the lateral neighboring lipid in the DPhPC bilayer. On the other hand, such structure is seldom found in the DPPC bilayer.

Figure 3c plots distributions of the chain length for both lipids. This figure shows that the branched chain is shorter than the straight one. The length of the chain is closely related to the gauche ratio of the dihedral angles in the chain. As shown in Table 1, a larger number of gauche conformers were observed in DPhPC than in DPPC. The average lengths of the chain vectors were 14.9 and 14.1 Å for DPPC and DPhPC, respectively. The difference accounts for the difference in membrane thickness.

3.3. Chain Conformation and Dynamics. The conformational disorder of the hydrophobic chain will be related to the bilayer stability under mechanical stress. The lipid conformational order is much lower in the liquid-crystal state than in the gel or crystal state. To characterize the segmental order of the lipid chain, the ^{2}H NMR order parameter was conventionally used. The order parameter can be evaluated by molecular simulations using the following definition:

$$S_{CD} = \frac{1}{2}\langle 3\cos^2\theta - 1\rangle$$

where θ is the angle between the C−D bond vector and the bilayer normal. The brackets denote an averaging over all lipids and time. The order parameter profiles along the chain for DPPC and DPhPC bilayers are shown in Figure 5. The calculated order parameter for DPPC molecules showed good agreement with that obtained by the NMR measurement.[22] In the case of the straight chain, the profile is characterized by a high-order plateau region in the middle of the chain and relatively disordered tail and ester regions. The disorder of the ester region is due to the reorientation of the chain at the segments. DPhPC showed a stepwise order parameter profile along the chain. All these steps in the profile were located at the carbon where the methyl branch was linked. This was also observed in the previous MD calculation.[20] The profile obtained for DPhPC was slightly lower throughout the chain than was the profile for DPPC. Thus, the branching reduced not only the orientational order but also the segmental order of the chain. The order parameters of the branched methyl group in the DPhPC molecule have small positive values, which were also observed in the previous MD calculation.[20]

To characterize the conformations of the hydrophobic chains, the probability of the gauche conformer along the main chains was also analyzed. This is plotted as a function of carbon number in Figure 6a. A high probability of gauche conformers was clearly observed in the vicinity of the branched carbons (C3, C7, C11, C15) of DPhPC molecules. This can be explained by the fact that the two dihedral states, gauche and trans, are energetically almost equivalent due to the steric repulsion of the branched methyl group. The gauche conformers in the vicinity of *tert*-carbons give rise to reorientation of the chain. On the other hand, the two dihedrals located between the *tert*-

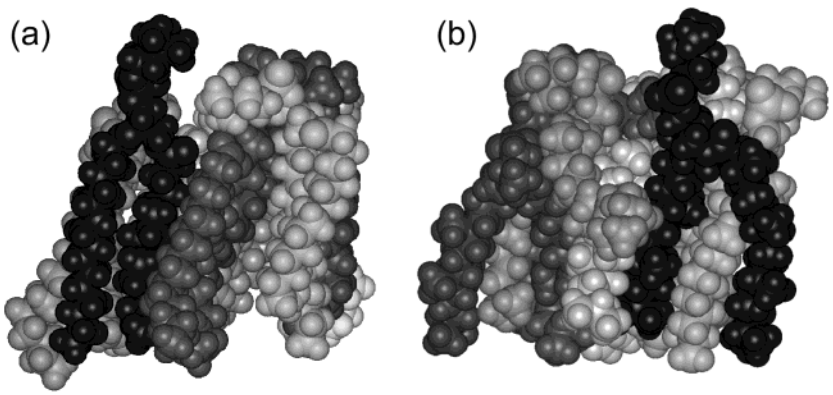

Figure 4. Typical snapshots of the lipid membrane patches. (a) DPPC and (b) DPhPC.

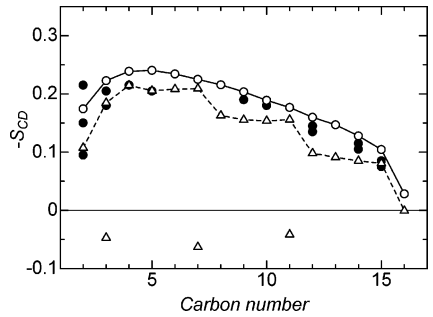

Figure 5. Order parameter profiles along the main chain. Open circles, DPPC; open triangles, DPhPC; filled circles, DPPC ^{2}H NMR measurement at 323 K.[22] The calculated profiles are the average of the two (*sn*-1 and *sn*-2) chains.

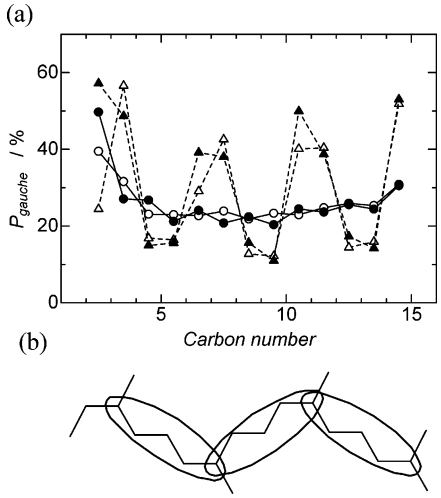

Figure 6. (a) Ratio of gauche conformers as a function of carbon number along chains. Filled circles, *sn*-1 chain of DPPC; open circles, *sn*-2 chain of DPPC; filled triangles, *sn*-1 chain of DPhPC; open triangles, *sn*-2 chain of DPhPC. (b) A likely found conformation of the highly branched phytanoyl chain.

carbons showed a higher probability of trans conformers than did the straight-chained counterparts. Thus, the highly branched phythanoyl chain tends to bend selectively at the dihedrals in the vicinity of *tert*-carbons, as is schematically drawn in Figure 6b. The bend of the chain promotes the intersection among the neighboring chains in the membrane layers. As shown in the snapshot of the DPhPC in Figure 4, some branched chains were caught between the two chains of the neighboring lipid. It is expected that such a structural correlation between the lipid chains slows down the conformational motion.

We now turn our attention to the dynamics of the chains. The rate of trans−gauche isomerization of the dihedral angles was evaluated using the following state function $S(t,\phi)$:

$$S(t,\phi) = \begin{cases} 1 & (\phi \geq (2/3)\pi, \text{ trans state}) \\ -1 & (\phi < (2/3)\pi, \text{ gauche state}) \end{cases}$$

This function describes the state of the dihedral angle ϕ at time t. The relaxation time of the autocorrelation function, $C(t)$, of the state function gives a measure of the net isomerization rate.

$$C(t) = \frac{\langle \delta S(t)\, \delta S(0) \rangle}{\langle \delta S(0)^2 \rangle}$$

where

$$\delta S(t) = S(t) - \langle S \rangle$$

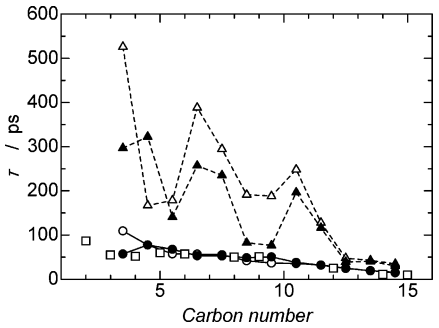

Figure 7. Trans−gauche isomerization rate: relaxation time profile as a function of carbon number. Filled circles, *sn*-1 chain of DPPC; open circles, *sn*-2 chain of DPPC; filled triangles, *sn*-1 chain of DPhPC; open triangles, *sn*-2 chain of DPhPC. The NMR relaxation time of segmental CD vectors of DPPC (open squares) is also plotted.[23]

The relaxation time was estimated by the numerical integration of the correlation function, $C(t)$, and a correction for the larger time was made by fitting the tail region of the function to a single-exponential function. The relaxation time is plotted against the carbon number along the chain in Figure 7. For the straight-chained DPPC, the NMR relaxation time of segmental CD vectors is also presented in the figure.[23] As was the case in our previous MD study,[16] in which a united-atom OPLS force field was used, in the present study the calculated profile of the relaxation time was similar to that obtained by NMR, though the NMR relaxation time reflects not only fast trans−gauche isomerization but also slow motions, such as the axial rotation and fluctuation of a lipid molecule. The branched DPhPC showed a significantly longer relaxation time profile throughout the chain. Since the fluidity of the chain was largely characterized by the rotation of the dihedral angle, the slower isomerization of the branched DPhPC would give rise to the slower wobbling of the chain and the slower rotation of DPhPC as compared with DPPC. The difference between the *sn*-1 and *sn*-2 chains of the DPhPC molecules may stem from the statistical errors due to the short MD time (and the slow dynamics of the chain).[24] It was clearly shown, however, that the branched chain was less mobile than the straight one: for the middle part of the chains, the relaxation time of the correlation function of DPhPC was approximately 5 times that of DPPC. The peaks of DPhPC occurred at the *tert*-carbon in the relaxation time profile. The same was also observed in the ^{13}C NMR relaxation time profile.[25] The long-lived bending conformation of the branched chain at the *tert*-carbons could be a result of chain entrapment between the neighboring lipids. A relaxation time in the range of 200−300 ps observed for the middle part of the branched chain was comparable to that of dihedrals around glycerol groups in the DPPC molecule.[16]

3.4. Water Penetration. Because DPPC and DPhPC have the same headgroup (phosphatidylcholine), the local hydration structure of the headgroups was largely unchanged. We have calculated the radial distribution function (RDF) between water oxygen and phosphorus or nitrogen. The difference in RDF between the DPPC and DPhPC bilayers was trivial. However, since DPhPC has an approximately 18% larger cross-sectional area, a larger amount of hydrating water does exist at the interfacial region. To study water penetration into the bilayers, a probability distribution of water molecules along the bilayer normal was plotted as shown in Figure 8a. In the plot, the origin of the abscissa, the bilayer normal pointing toward the outside of the bilayer, was chosen at the averaged position of phosphorus atoms. In both lipid bilayers, no water molecule penetrated beyond the positions of the carbonyl carbons (not shown in the

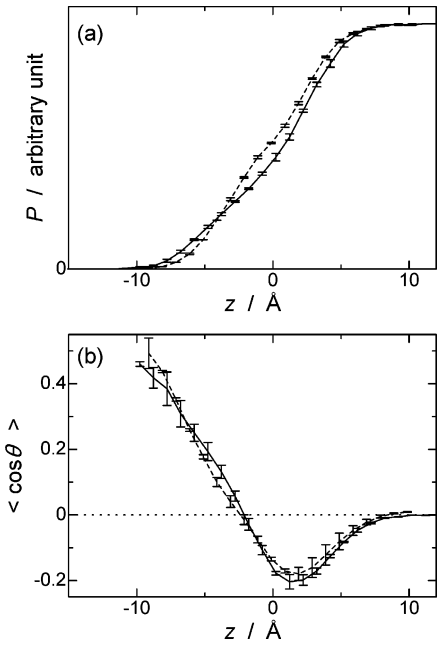

Figure 8. (a) Probability distribution of water molecules along the bilayer normal. (b) Averaged orientation of water along the bilayer normal. Solid lines, DPPC; dashed lines,DPhPC. θ is the angle between the water dipole axis and the bilayer normal.

figure). A larger amount of water molecules inhibited near the phosphorus ($z = 0$) was observed for DPhPC as a result of its larger cross-sectional area. This finding is in harmony with the experimental observation that degree of water penetration near the membrane/water interface is higher in the DPhPC bilayer than in straight-chained lipid bilayers.[6] The averaged orientational distribution of the water dipole with respect to the bilayer normal was calculated using the following function:

$$\langle \cos\theta \rangle_{z=z'} = \langle \vec{\mu} \cdot \vec{n} \rangle_{z=z'}$$

where $\vec{\mu}$ is the normalized water dipole vector, $\vec{n}$ is the bilayer normal pointing outside of the membrane, and the brackets denote averaging over all water molecules in the slab ($\Delta z = 1$ Å) and over time. The calculated distributions are plotted in Figure 8b. The abscissa was taken to be the same as in Figure 8a. The orientational distribution of the water was almost identical between the DPPC and DPhPC bilayer systems. It was clear that, in the interfacial region, the water orientation was highly correlated with the position of the phosphorus: a water dipole tends to point toward the phosphorus.

Next, the lifetime of the phosphate-bound water was estimated. The bound water is defined as locating in the first salvation shell of the phosphorus. The state function of water is defined as follows:

$$W(t) = \begin{cases} 1 & \text{(if the water locates in the first} \\ & \quad \text{hydration shell of the phosphorus)} \\ 0 & \text{(otherwise)} \end{cases}$$

The autocorrelation function of the state function

$$C(t) = \frac{\langle W(t)\, W(0) \rangle}{\langle W(0)\, W(0) \rangle} = \frac{1}{N_{\mathrm{hyd}}} \langle W(t)\, W(0) \rangle$$

was used to estimate the exchange rate of the water molecules. The function $C(t)$ showed a single-exponential decay for both lipid bilayer systems. The relaxation time was calculated to be 9.0 ± 0.7 and 7.1 ± 0.3 ps for the DPPC and DPhPC bilayer systems, respectively. The shorter lifetime of the bound water for DPhPC systems can be related to the larger amount of boundary water due to the expansion of the cross-sectional area. The shorter lifetime suggested higher mobility of water at the interface and indirectly suggested a faster torsional motion of the headgroup. Thus, chain branching decreases the rate of trans−gauche isomerization of the hydrophobic chain itself, but not that of the headgroup.

4. Conclusions

A comparison of the DPPC and DPhPC bilayers for the static and dynamic properties has been made to investigate the effect of chain branching on bilayer stability. In the branched chain, gauche conformers were probably observed at the dihedrals in the vicinity of *tert*-carbons, which brought about the selective chain bending at the branched segments. The characteristic conformation of the branched chain decreased the probability of parallel chains in a lipid. In addition, the branched chains tend to be interposed with the two chains of the lateral neighboring lipid and, as a consequence, the branched chain showed a much lower overall rate of trans−gauche isomerization than its straight counterpart. We conclude that the higher structural stability of the branched DPhPC bilayer is attributable to the slower conformational motion of the hydrophobic chain, which is clearly correlated with the observed chain entrapment between lateral neighboring lipid molecules.

Acknowledgment. This work was partly supported by NAREGI Nanoscience Project, Ministry of Education, Culture, Sports, Science and Technology, Japan.

References and Notes

(1) *The Structure of Biological Membranes*; Yeagle, P., Ed.; CRC Press: Boca Raton, FL, 1991. *Permeability and Stability of Lipid Bilayers*; Disalvo, E. A., Simon, S. A., Eds.; CRC Press: Boca Raton, FL, 1995.

(2) Driessen, A. J. M.; van de Vossenberg, J. L. C. M.; Konings, W. N. *FEMS Microbiol. Rev.* **1996**, *18*, 139. Gambacorta, A.; Gliozzi, A.; de Rosa, M. *World J. Microbiol. Biotechnol*. **1995**, *11*, 115.

(3) Minamikawa, H.; Hato, M. *Langmuir*, **1997**, *13*, 2564. Minamikawa, H.; Hato, M. *Langmuir* **1998**, *14*, 4503.

(4) Baba, T.; Minamikawa, H.; Hato, M.; Motoki, A.; Hirano, M.; Zhou, D.; Kawasaki, K. *Biochem. Biophys. Res. Commun*. **1999**, *265*, 734.

(5) Baba, T.; Toshima, Y.; Minamikawa, H.; Hato, M.; Suzuki, K.; Kamo, N. *Biochim. Biophys. Acta* **1999**, *1421*, 91.

(6) Baba, T.; Minamikawa, H.; Hato, M.; Handa, T. *Biophys. J*. **2001**, *81*, 3377.

(7) Lindsey, H.; Petersen, N. O.; Chan, S. I. *Biochim. Biophys. Acta* **1979**, *555*, 147.

(8) Taylor, R. J.; de Levie, R. *Biophys. J*. **1991**, *59*, 873.

(9) MacKerell, A. D., Jr.; Bashford, D.; Bellott, M.; Dunbrack, R. L., Jr.; Evanseck, J. D.; Field, M. J.; Fischer, S.; Gao, J.; Guo, H.; Ha, S.; Joseph-McCarthy, D.; Kuchnir, L.; Kuczera, K.; Lau, F. T. K.; Mattos, C.; Michnick, S.; Ngo, T.; Nguyen, D. T.; Prodhom, B.; Reiher, W. E., III; Roux, B.; Schlenkrich, M.; Smith, J. C.; Stote, R.; Straub, J.; Watanabe, M.; Wiorkiewicz-Kuczera, J.; Yin, D.; Karplus, M. *J. Phys. Chem. B* **1998**, *102*, 3586.

(10) Jorgensen, W. L.; Chandrashekar, J.; Madura, J. D.; Impey, R.; Klein, M. L. *J. Chem. Phys*. **1983**, *79*, 926.

(11) Allen, M. P.; Tildesley, D. J. *Computer Simulation of Liquids*; Clarendon Press: Oxford, UK, 1987.

(12) Pearson, R. H.; Pascher, I. *Nature* **1979**, *281*, 499.

(13) Martyna, G. J.; Tuckerman, M. E.; Tobias, D. J.; Klein, M. L. *Mol. Phys.* **1996**, *87*, 1117.

(14) Tuckerman, M.; Martyne, G. J.; Berne, B. J. *J. Chem. Phys*. **1992**, *97*, 1990.

(15) Shinoda, W. Manuscript in preparation.

(16) Shinoda, W.; Namiki, N.; Okazaki, S. *J. Chem. Phys*. **1997**, *106*, 5731.

(17) Nagle, J. F.; Zhang, R.; Tristram-Nagle, S.; Sun, W.; Petrache, H. I.; Suter, R. M. *Biophys. J*. **1996**, *70*, 1419.

(18) We, Y.; He, K.; Ludtke, S. J.; Huang, H. W. *Biophys. J*. **1995**, *68*, 2361.

(19) Mendelsohn, R.; Davies, M. A.; Brauner, J. W.; Schuster, H. F.; Dluhy, R. A. *Biochemistry* **1989**, *28*, 8934. Pink, D. A.; Green, T. J.; Chapman, D. *Biochemistry* **1980**, *19*, 349. Seelig, J.; Seelig, A. Q. *Rev. Biophys*. **1980**, *13*, 19.

(20) Husslein, T.; Newns, D. M.; Pattnaik, P. C.; Zhong, Q.; Moore, P. B.; Klein, M. L. *J. Chem. Phys*. **1998**, *109*, 2826.

(21) Note that the angular distribution function presented in Figure 7 of ref 20 may be a nonweighted function, *P*.

(22) Seelig, A.; Seelig, J. *Biochemistry* **1974**, *13*, 4839.

(23) Brown, M. F.; Seelig, J.; Häberlen, U. *J. Chem. Phys*. **1979**, *70*, 5045.

(24) Another 10 ns NVE-MD calculation suggested that a statistical error of the estimated relaxation time in Figure 7 was not larger than the difference between the two (*sn*-1 and *sn*-2) chains of DPhPC.

(25) Degani, H.; Danon, A.; Caplan, S. R. *Biochemistry* **1980**, *19*, 1626.